

- Science* **178**, 1087 (1972); U. Fink, N. H. Dekkers, H. P. Larson, *Astrophys. J. Lett.* **179**, L155 (1973).
8. U. Fink, H. P. Larson, T. N. Gautier, R. Trefers, *Astrophys. J. Lett.* **207**, L63 (1976).
  9. D. Morrison, D. P. Cruikshank, C. B. Pilcher, G. H. Rieke, *ibid.*, p. L213.
  10. T. V. Johnson, G. Veeder, D. L. Matson, *Icarus* **24**, 428 (1975).
  11. G. P. Kuiper (1956), quoted in D. L. Harris, in *Planets and Satellites*, G. P. Kuiper and B. M. Middlehurst, Eds. (Univ. of Chicago Press, Chicago, 1961), p. 305.
  12. Laboratory spectra were supplied by H. H. Kieffer.
  13. M. J. Gaffey, *J. Geophys. Res.* **81**, 905 (1976).
  14. C. R. Chapman and J. W. Salisbury, *Icarus* **19**, 507 (1973); C. R. Chapman and D. Morrison, *ibid.* **28**, 91 (1976).
  15. Kitt Peak National Observatory is operated by the Association of Universities for Research in Astronomy, Inc., under contract with the National Science Foundation. The authors were visiting scientists at the observatory when this work was performed.
  16. F. J. Low and G. H. Rieke, in *Methods Exp. Phys.* **12** (part A), 415 (1974); H. L. Johnson, *Annu. Rev. Astron. Astrophys.* **4**, 193 (1966).
  17. G. P. Kuiper, *Commun. Lunar Planet. Lab.* **2**, 17 (1963).
  18. H. H. Kieffer, *J. Geophys. Res.* **75**, 501 (1970).
  19. W. D. Smythe, *Icarus* **24**, 421 (1975).
  20. L. Andersson and J. D. Fix, *ibid.* **20**, 279 (1973).
  21. G. P. Kuiper, *Trans. Int. Astron. Union* **9**, 250 (1954).
  22. I. Halliday, R. H. Hardie, O. G. Franz, J. B. Priser, *Publ. Astron. Soc. Pac.* **78**, 113 (1966).
  23. R. L. Duncombe, P. K. Seidemann, W. J. Klepczynski, *Fundam. Cosmic Phys.* **1**, 119 (1974); *Annu. Rev. Astron. Astrophys.* **11**, 135 (1973).
  24. M. E. Ash, I. I. Shapiro, W. B. Smith, *Science* **174**, 551 (1971).
  25. C. W. Tombaugh, in *Planets and Satellites*, G. P. Kuiper and B. M. Middlehurst, Eds. (Univ. of Chicago Press, Chicago, 1961), p. 12.
  26. We thank R. Joyce and R. Capps for assistance with the photometric equipment, and G. Consolmagno and I. I. Shapiro for useful conversations. This work was supported in part by grant NGL 12-001-057 from the National Aeronautics and Space Administration.

25 June 1976; revised 3 September 1976

## Increased Transport of Antarctic Bottom Water in the Vema Channel During the Last Ice Age

**Abstract.** Particle size analyses of surface sediments in the Vema Channel reveal a spatial variation related to the present hydrography. Similar analyses of sediment deposited during the last ice age (18,000 years before the present) indicate a maximum shallowing of the upper limit of Antarctic Bottom Water (AABW) of about 100 meters, coupled with an increase in velocity, which resulted in an increase in AABW transport.

The Vema Channel (Fig. 1) is a narrow gap in the Rio Grande Rise through which Antarctic Bottom Water (AABW) flows northward from the Argentine Basin into the Brazil Basin (1). It has been the major path of AABW flow since the Pliocene before which the Hunter Channel to the east (2) may have been a more important route (3). There is evidence that the Vema Channel is an erosional

feature created by the high-velocity northward flow of AABW through the constriction of the gap (1). Average bottom current velocities observed in the axis of the channel are 20 to 25 cm/sec (4). Flume studies suggest that such bottom current velocities are sufficient to cause scour in deep-sea sediments (5), especially if microrelief such as manganese nodules is present (6). We attempt here

to identify the extent of AABW in the Vema Channel during the last glacial period.

Two water masses are present in the Vema Channel, the deeper northward-flowing AABW and the shallower North Atlantic Deep Water (NADW) which flows south with a lower velocity (1). The transition zone between the two water masses is marked by sharp gradients in water properties and in the concentration of suspended particulates (4), and by pronounced changes in the characteristics of the underlying sediments (7). The identification of the level of no motion (LNM) within this transition zone is somewhat arbitrary in the absence of closely spaced observations of current. Hydrographic considerations (4) suggest that the LNM may correspond approximately with the 1.2°C potential temperature isotherm, a surface which in turn corresponds to the foraminiferal lysocline at approximately 4000 m on the east flank of the channel (7, 8). An alternative interpretation, more consistent with data presented here, is that the LNM corresponds to the maximum gradient in the benthic thermocline, which slopes from about 3900 to 4000 m on the western side of the channel to about 4200 to 4250 m on the eastern side (4).

Where the LNM intersects the sea floor one would expect to find a stagnation zone produced by the effect of opposing currents (9). Although this zone may be characterized by turbulent conditions, the net advective component should be approximately zero so that bottom current transport of sediment should be minimal. This effect should result in a

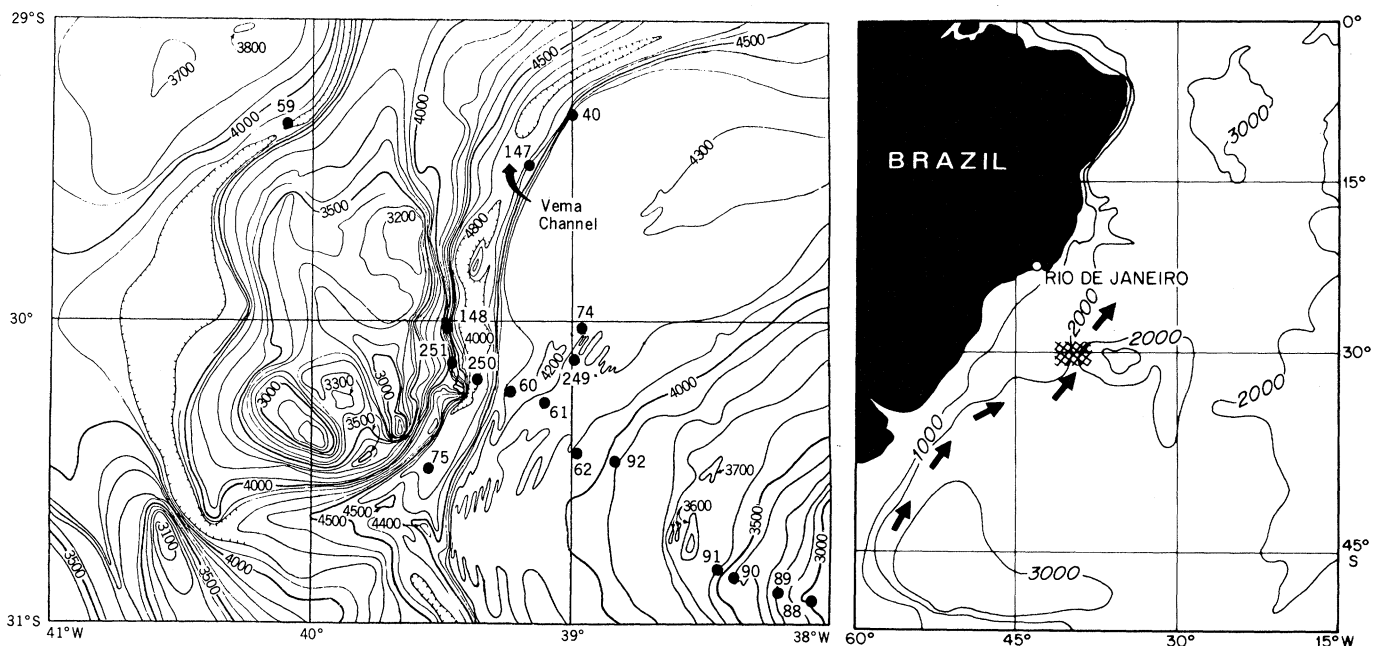


Fig. 1. (Left) Map showing the location of cores (Chain 115-60, 61, 62, 88, 89, 90, 91, 92; Vema 22-74, 75; Vema 24-249, 250, 251; Robert Conrad 11-40; Robert Conrad 15-147, 148) in the Vema Channel. Bathymetry (in meters, corrected for the density of the water) is from (4). (Right) Regional setting of the Vema Channel in the southwestern Atlantic.

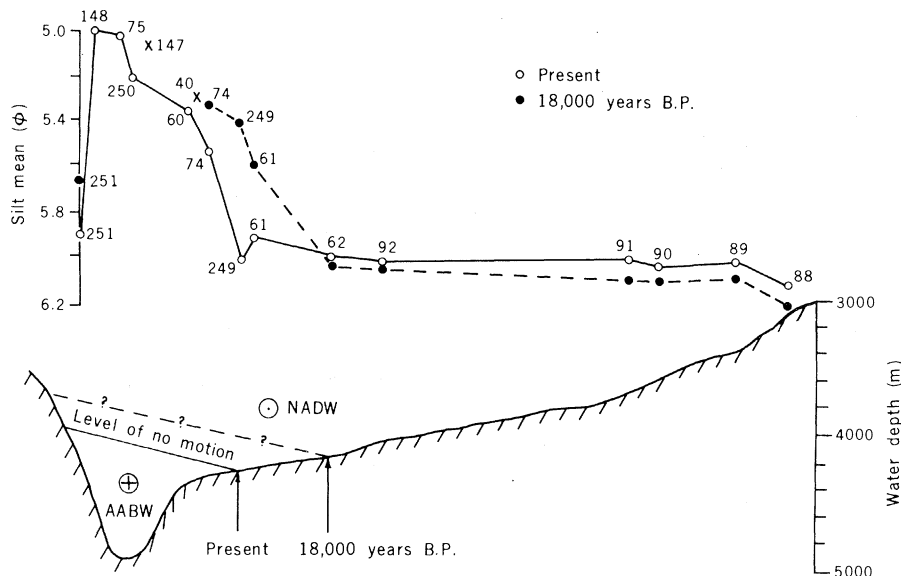


Fig. 2 (Bottom). East-west profile of the Vema Channel with deeper AABW flowing north ( $\oplus$ ) and shallower NADW flowing south ( $\ominus$ ). The present level of no motion was chosen to correspond with the maximum gradient of the benthic thermocline (—) and the LNM 18,000 years B.P. (- - -) determined in this study (see text). (Top) Silt mean in  $\phi$  units (the negative logarithm to the base 2 of the grain size in millimeters). Cores are plotted relative to position on the bathymetric profile below. The silt mean on the present sea floor ( $\circ$ ) is from trigger core-top samples; the silt mean in the samples 18,000 years B.P. ( $\bullet$ ) were chosen from  $^{18}\text{O}$  and  $\text{CaCO}_3$  curves (13). The silt mean in core-top samples of cores 40 and 147 (shown by  $\times$ ) are north of the profile of the other cores (Fig. 1) but are added for comparison.

zone with higher sedimentation rates and finer-grained sediment preferentially deposited under less dynamic bottom current conditions.

In principle, the effect of current scour should be most pronounced in the axis of the channel where bottom current velocities are highest, whereas near the edges of the flow the velocity should be sufficiently diminished that scouring is replaced by selective winnowing. The result would be a change in the sizes of particles deposited as a function of position in the channel. The relationship between particle size distribution and relative bottom current velocity in winnowing zones suggests that higher bottom current velocities are marked by coarser sediment resulting from the selective removal of the finer fraction (10). Therefore, the particle size distribution should be a sensitive monitor of relative bottom current velocities, with finer mean particle size interpreted as an indication of relatively lower velocity. We have used this procedure to interpret the lateral extent of fast-flowing AABW in the Vema Channel (7).

We have examined the relationship between the present hydrography and the surface sediment in a series of trigger core-top samples from the eastern flank of the channel (Fig. 1). A comparison of the mean particle size in the silt fraction of carbonate-free sediment (11) and the hydrography is presented in Fig. 2. The silt mean on the present sea floor varies only slightly in cores 88 through 249 and

represents the finest mean values of silt size, suggesting a relatively low velocity for NADW. The sharp change in the mean size of silt particles west of core 249 is due to a coarsening of the silt fraction, an effect that may be due to intense winnowing of fine particles by high-velocity AABW. The region of maximum values of the silt mean clearly defines a zone of high-velocity AABW. The coarsest sediment is found in core 148 (Fig. 2) on the western slope of the channel, which is expected as a result of a westward intensification of north-flowing bottom currents in the Southern Hemisphere. The finer silt mean in core 251 (Fig. 2) suggests that this core may be near the LNM on the western side of the channel. This interpretation is supported by the fact that the present benthic thermocline is slightly shallower than that core (Fig. 2). Since the sediment in core 251 is not as fine as that in core 249, we suggest that the LNM may be west of, and shallower than, core 251.

Critical to estimating paleotransport in the Vema Channel is the selection of an isochron along which the particle size distribution may be determined and compared with that of present-day sediments. The peak of the last ice age at 18,000 years before the present (B.P.) was chosen from oxygen isotope stratigraphy in two of the cores (12) and total carbonate analysis (7, 13) in all the cores. High-velocity AABW has caused scour or intense winnowing on the sea floor deeper than 4250 m, and con-

sequently the level corresponding to 18,000 years B.P. cannot be identified in cores deeper than that level. However, cores under AABW shallower than 4200 m (for example, cores 74, 249, and 61 in Fig. 2) and all cores recovered under NADW may be correlated on the basis of the isochron at 18,000 years B.P.

The distribution of the silt mean on the sea floor during the last ice age (Fig. 2) differs significantly from that at present. The upper limit of the zone of high silt mean values, for which we infer high-velocity AABW flow, was shallower by 100 m (that is, to the location of core 62, Fig. 2). This suggests that the top of the fast-flowing AABW shallowed by approximately 100 m in the Vema Channel during the last ice age. The silt mean under NADW 18,000 years B.P. has a spatial variation similar to but finer than that of the present, suggesting a similar flow profile with a somewhat lower velocity. This evidence suggests that the increased flow of AABW during the last glacial maximum was not matched by an increased production of bottom water in the North Atlantic (14).

The volume transport of AABW in the channel is controlled by the position of the LNM and by the mean velocity of AABW through a cross section bounded by the LNM and the channel walls. Estimates of present AABW transport in the Vema Channel have differed depending on the cross section selected and the computed velocity profile (1, 4). In principle, however, changes in the relative transport may be estimated from spatial and down-core analysis of the particle size distribution of the silt fraction.

Examination of Fig. 2 shows that, without any increase in the velocity of AABW during the last ice age, the transport of bottom water was at least 20 percent greater because of the shallowing of the LNM and thereby an increase in the cross-sectional area of AABW flow (15). If the velocity of AABW also increased, then the increased transport would be greater than this minimum estimate. The relative increase in the velocity of AABW during the last ice age may be estimated from a single core which was under AABW both at present and 18,000 years B.P. Cores under AABW but near the LNM (for example, cores 249 and 61 in Fig. 2) will not be reliable indicators of the magnitude of the velocity increase since only small changes from the "no motion" state may cause large variations in the silt mean which will give a false impression of magnitude changes. Core 74 near the eastern edge of AABW and core 251 near the western edge meet the above criterion since they are far enough from the edge effects of AABW but not

so deep that winnowing or erosion has left large gaps in the sedimentary record.

It is clear that the silt mean in cores 74 and 251 during the last ice age was coarser than at present (Fig. 2), an indication of a higher current velocity 18,000 years B.P. It is not possible to interpret the silt mean as a simple function of bottom current velocity; however, the relative increase in particle size in both cores may be used to infer a relative increase in velocity. In core 74 the silt mean 18,000 years B.P. is  $5.3 \phi$  compared to the present silt mean of  $5.5 \phi$ . The silt mean coarsened from  $5.9 \phi$  to  $5.65 \phi$  in core 251 during the last ice age. The magnitude of the change in the silt mean is nearly the same in both cores; this finding suggests a similar relative increase in bottom current velocity on both sides of the channel. Therefore, the particle size data suggest an increase in AABW velocity during the last ice age, although we cannot estimate the magnitude of the change.

Particle size analysis of sediment from 18,000 years B.P. indicates that the combined effects of a shallower LNM and possibly increased velocity of bottom water resulted in an increase in AABW transport through the Vema Channel during the last glacial maximum. Our approach has provided a semiquantitative method by which to interpret changes in bottom water production during the past. If demonstrated to be worldwide in extent, this increased transport conceivably could be the cause of widespread erosional disconformities which have been suspected to be associated with Neogene glaciations (16).

MICHAEL T. LEDBETTER

Graduate School of Oceanography,  
University of Rhode Island, Kingston

DAVID A. JOHNSON

Woods Hole Oceanographic Institution,  
Woods Hole, Massachusetts

#### References and Notes

1. X. Le Pichon, M. Ewing, M. Truchan, *Phys. Chem. Earth* **8**, 31 (1971).
2. L. H. Burckle and P. E. Biscaye, *Geol. Soc. Am. Abstr. Programs* **3**, 518 (1971).
3. H. B. Zimmerman et al., *Eos* **57**, 256 (1976).
4. D. A. Johnson, S. E. McDowell, L. G. Sullivan, P. E. Biscaye, *J. Geophys. Res.*, in press.
5. J. B. Southard, R. A. Young, C. D. Hollister, *ibid.* **76**, 5903 (1971).
6. P. Lonsdale and J. B. Southard, *Mar. Geol.* **17**, M51 (1974).
7. D. A. Johnson, M. T. Ledbetter, L. H. Burckle, *ibid.*, in press.
8. M. Melguen and J. Thiede, *ibid.* **17**, 341 (1974).
9. T. A. Davies and A. S. Laughton, in *Initial Reports of the Deep-Sea Drilling Project, Leg 12* (Government Printing Office, Washington, D.C., 1972), p. 905.
10. T. C. Huang and N. D. Watkins, *Mar. Geol.*, in press.
11. In the particle size analysis we used a Coulter Counter (model ZB). The particle size distribution of the total silt fraction is a function of many factors. In order to reduce the number of variables affecting that distribution, the carbonate was removed prior to size analysis (the effects of carbonate dissolution upon the resulting particle size distribution were thus removed). Fluctua-

- tions in the silt mean in the carbonate-free sediment may be interpreted in many ways but in a high-velocity regime the redistribution of these fine particles by bottom currents is certainly a major cause.
12. C. S. Peters, *Woods Hole Oceanog. Inst. Tech. Rep.* 76-10 (1976).
13. Oxygen isotope analyses (12) and total carbonate analyses were carried out on samples from the same levels in cores 88 and 89, which were dated with paleomagnetic stratigraphy (7). The linear correlation coefficient between the two variables is  $-0.508$  (core 88) and  $-0.509$  (core 89). Therefore, interglacials are characterized by high carbonate and glacial by low carbonate. The final maximum of the last ice age corresponds to the last maximum in ice volume [N. J. Shackleton and N. D. Opdyke, *Quat. Res. (N.Y.)* **3**, 39 (1973)] which is correlated with the most recent carbonate low in every core.
14. J. C. Duplessy, L. Chenouard, F. Vila, *Science* **188**, 1208 (1975).

15. When computing the change in cross-sectional area 18,000 years B.P., we assumed that the LNM had the same slope as at present.
16. N. D. Watkins and J. P. Kennett, *Antarct. Res. Ser.* **19**, 273 (1972); D. A. Johnson, *Geol. Soc. Am. Bull.* **83**, 3121 (1972); *Mar. Geol.* **17**, 71 (1974); J. P. Kennett and N. D. Watkins, *Geol. Soc. Am. Bull.* **87**, 321 (1976); T. A. Davies, O. E. Weser, B. P. Luyendyk, R. B. Kidd, *Nature (London) Phys. Sci.* **253**, 15 (1975).
17. We thank N. D. Watkins and T. C. Moore for critical review. We are grateful for the use of the Lamont-Doherty Geological Observatory core collection maintained under NSF grant DES 72-01568 and ONR grant N00014-75-C-0210. M.T.L. was supported by NSF grant DES 75-13839 and ONR grant N00014-76-C-0226. D.A.J. was supported by NSF grant OCE 74-01744. Contribution No. 3823 of the Woods Hole Oceanographic Institution.

2 July 1972; revised 4 August 1976

## Appearance of Vegetation in Ultraviolet Light: Absorbing Flowers, Reflecting Backgrounds

**Abstract.** *Flowers that uniformly absorb ultraviolet light may contrast strikingly with a bright ultraviolet-reflecting background, such as densely hairy or glaucous foliage, white soils, or the sky. Shadows will not resemble these flowers if the appearance of each in visible light is also considered. Examples are shown from Mexican heliotropiums and Michigan dune plants.*

Since the realization that insects use ultraviolet (UV) reflectance patterns in searching for flowers, such patterns have been extensively studied (1). However, little note has been taken of the background against which the flowers are normally viewed. Usually the background is tacitly assumed to absorb UV light, and published photographs generally have dark gray or black backgrounds. Thus, flowers that do not reflect UV seem uninteresting. In fact, some natural backgrounds are highly reflectant of UV, and flowers that absorb UV contrast strikingly with them.

To facilitate interpretation of photographs taken with visible (to the human eye) and UV light, I equalized the contrast and standardized the exposures, so that equal percentages of reflectances result in approximately equally bright images (2). In the pictures taken with ringflash illumination (3) the distant background appears to be black as a result of the rapid decrease of light intensity with increasing distance from the flash; however, the brightness of objects near the focal plane can be compared. The pictures taken with daylight illumination show much more realistic appearances.

I first encountered the pattern of a dark flower against a bright background in Mexico during a study of *Heliotropium* section *Orthostachys* and sect. *Halmyrophila*. The small flowers of these plants are positioned close to the leaves so that a plant's foliage constitutes much of its flower's background. In visible light these flowers are white with a yellow or yellow-green center. The densely

hairy or glaucous leaves, stems, sepals, and bracts are whitish-green or green. Most of these species have UV images showing dark flowers and bright foliage. An animal whose color vision includes UV will see the flower as a brightly colored spot rich in visible light and poor in UV. The foliage will appear white or pastel owing to its high reflectance at all wavelengths (Figs. 1 and 2).

Some plants that expose part of the back of the corolla in bud have a UV pattern that looks like sepals on the early exposed corolla parts and one that looks like a flower on the parts exposed at opening. In other examples (4) the sepals were UV-absorbing and the flower was mostly reflecting. Some species of *Heliotropium* show the same phenomenon but with the colors reversed. Here a row of hairs makes the early exposed rear portions of the corolla highly reflectant in the UV, while the hairless remainder is dark (Figs. 3 and 4). On the foliage as well, the hairs (or glaucous covering) are responsible for the bright UV reflection. The actual leaf surface reflects little UV.

Since sand provides a UV-reflecting background, I took photographs of sand dune vegetation near Lake Michigan in the hope of finding more plants with the dark-flower UV pattern. A number of additional examples were found and three are shown (Figs. 5-7). The dune pictures were taken with daylight illumination on sunny days and so include shadows. The shadows are less depleted of UV light than of visible light, since the very bright UV from the "blue" sky partly fills in the sunlight shadows. Therefore, the